coatings

Article

Characterization and Wear Response of Magnetron Sputtered W–B and W–Ti–B Coatings on WC–Co Tools

Joanna Radziejewska [1,2], Rafał Psiuk [1] and Tomasz Mościcki [1,*]

1 Institute of Fundamental Technological Research, Polish Academy of Science, 5B Pawinskiego St., 02-106 Warsaw, Poland; jradz@ippt.pan.pl (J.R.); rpsiuk@ippt.pan.pl (R.P.)
2 Faculty of Production Engineering, Warsaw University of Technology, 85 Narbutta St., 02-524 Warsaw, Poland
* Correspondence: tmosc@ippt.pan.pl; Tel.: +48-22-826-12-81

Received: 18 November 2020; Accepted: 14 December 2020; Published: 16 December 2020

Abstract: In this work, α-WB_2 and $(W,Ti)B_2$ borides were applied as wear-resistant coatings to commercial WC–Co cutting inserts. Properties of coatings deposited by magnetron sputtering on WC–Co tools were studied. The crystal structure and chemical composition were analyzed. Vickers hardness and surface roughness were determined and wear test in semi-dry conditions was performed. The W–B and W–Ti–B coatings deposited on WC–Co substrate were smooth and very hard. However, titanium alloy W-B films with Vickers hardness of 3630 ± 260 $HV_{0.02}$ were characterized by lower adhesion to the substrate, influencing the wear mechanism. Turning tests carried out on 304 stainless steel showed that the W–B film caused less wear compared to uncoated insert. Moreover, when W–B coating was applied, flank wear was reduced by 30% compared to uncoated WC–Co insert. Additionally, coating prevented chipping of the edge during cutting under test conditions. The research shows that W–B film deposited by magnetron sputtering has great potential as a coating for cutting tools for difficult-to-cut materials.

Keywords: PVD coatings; wear resistance; transition metal borides; cutting tools

1. Introduction

New tool materials or coatings are needed for special applications, particularly in machining of difficult-to-machine materials [1]. Coatings should be characterized by hardness, strength, and chemical inertness. Such properties are exhibited by boride films [2–7]. There are numerous compounds with boron that have good wear resistance, such as ZrB_2, TiB_2, BN, and Ti(B,N) [8]. In addition, tungsten borides and ternary transition (TM) metal-diborides possess very high application potential. The ternary TM-diboride coating films showing exceptionally high phase stability and mechanical properties, even at high temperature or even after exposition to high temperatures [2]. Addition of TM such as Ta or Ti cause that coatings possess fracture toughness k_{IC} (~3.5 MPa$\sqrt{m}$) higher than well-known coatings such us (Ti,Al)N, CrN/TiN, Ti–Si–N, TiN, and TiB_2 and at the same time they are super hard $H > 40$ GPa [2]. So far, there has been no research on the behavior of such layers under operating conditions. In Ref. [9] a series of borides (CrB_2, Mo_2B_5 and WB) were applied as protective coatings on cutting tools. Turning tests carried out on titanium in dry conditions showed that WB crystalline coating was resistant to abrasive wear. Similar properties were observed by Chrzanowska-Giżynska et al. [10,11], who investigated the friction coefficient and wear resistance of αWB coatings on flat stainless steel substrates in scratch tests. αWB films deposited by radio frequency magnetron sputtering (RF MS) were characterized by good adhesion. The 1 µm films tested in the scratch test failed at 200 mN due to cracking; however, further increase in the load did not cause spallation of the coating [10]. This study also indicated high wear resistance of 2.7×10^{-6} $mm^3 \cdot N^{-1} \cdot m^{-1}$ of such coatings.

Jiang et al. [12] showed that direct current magnetron sputtered (DC MS) αWB_2 coatings with a metastable AlB_2-type structure possessed a nanocomposite structure exhibiting superhardness of about 43.2 ± 5 GPa. In this case, the steady-state friction coefficient measured during sliding was 0.23. Additionally, the wear rate of the films was 6.5×10^{-6} $mm^3 \cdot N^{-1} \cdot m^{-1}$, indicating that AlB_2-type WB_2 coatings have good potential application as superhard and low-wear coatings. Moreover, TiB_2-coated tools compared to uncoated tools showed better wear resistance in the case of machining titanium alloy in rough turning conditions. However, it was stated that the efficiency of the coatings strongly depended on the cutting conditions [13].

Mixing tungsten and titanium borides causes other special features. For example, alloying tungsten boride coatings with titanium improved mechanical properties [4,14–18]. Euchner et al. [14] showed that films of solid solutions of $Ti_{1-x}W_xB_{2-z}$ deposited by magnetron sputtering (MS) over the whole composition range were crystallized in the AlB_2 structure type. The obtained coatings exhibited good thermal stability and high hardness with a maximum value of 40 GPa under 25 mN load for $Ti_{0.67}W_{0.33}B_{2-z}$ [14]. However, as shown in Ref. [19], nanocomposites can also be formed in regions with high tungsten content, which is optimal for achieving high strength. The maximum hardness (33 GPa under 70 mN load) was obtained for a nanocrystalline composite based on the phase $(Ti,W)B_2$ with Ti content of 10.2 at.%. A similar observation was made by Smolik et al. [20,21], who also studied the fracture toughness. Tungsten alloying of titanium diboride coatings shows that the addition of 10% of tungsten causes a more than seven-times increase in the fracture toughness K_{IC}, from $K_{IC(TiB_2)} = 0.67$ to $K_{IC(TiBW)} = 4.98$ $MPa \cdot m^{1/2}$. At the same time, Ti–B–W films were characterized by greater hardness (H = 38 GPa under 400 mN load) and similar surface roughness compared to TiB_2 coatings [20]. In both cases [14,20], films were deposited by DC magnetron sputtering.

Chrzanowska-Gizynska et al. [16] used a hybrid MS + pulsed laser deposition (PLD) method for doping of α-WB lattice with titanium. At a titanium content of 5.5 at.%, the hardness of titanium-doped coatings was 47–50 GPa under 2.5 mN load. Additionally, the titanium alloying resulted in a change in the α-WB structure to a mixed α-WB and AlB_2-type WB_2 structure. Such a high hardness was also reported by Moscicki et al. [4]. In this work, the authors studied the impact of titanium content on the properties of thin films deposited by RF magnetron sputtering from $W_{1-x}Ti_xB_{4.5}$ (where x = 0–0.24) spark plasma sintered targets. The results of the study showed that the addition of titanium apparently changed the film structure from nanocrystalline columnar to amorphous, a very dense and compact structure, with the addition of TiB_2 phase [4]. Deposited coatings with titanium content of 5.5 at.% were simultaneously hard (H > 37.5 GPa under 7 mN load) and had high hardness to effective Young's modulus ratio values (H/E^* > 0.1) and elastic recovery (W_e > 60%) appropriate for toughness and resistance to cracking materials [22]. $(W,Ti)B_2$ coatings with AlB_2 structure type also exhibited enhanced tribological and corrosive properties [4].

The described properties of $(W,Ti)B_2$ and α-WB_2 films indicate great potential for using them as protective coatings for cutting tools. So far, there has been no research on the behavior of such layers under operating conditions.

In this work, the above-mentioned borides (α-WB_2, $(W,Ti)B_2$) are applied as wear-resistant coatings to commercial WC–Co cutting inserts. Turning tests carried out on difficult-to-machine 304 stainless steel showed that the W–B film caused less wear compared to uncoated inserts. After cutting, test flank wear was examined. Such wear is often used to predict tool life and has a big influence on the accuracy of machining. The properties of boride films and the possibility of using boride coatings to protect WC–Co cutting tools for difficult-to-machine materials were studied.

2. Experimental Procedure

The sputtering target was made by spark plasma sintering (SPS) from boron powder (~625 mesh, 99.7% purity; Sigma Aldrich, St. Louis, MO, USA), tungsten (12 μm, 99.9% purity; Sigma Aldrich), and titanium (45 μm, 99.98% purity; Sigma Aldrich). For deposition of α-WB_2 film, powder was mixed and sintered with a 4.5:1 (B/W) ratio [23]. In the case of the target with titanium alloy, the ratio of boron to transition metals was 4.5 and Ti/(Ti + W) = 0.16 [4]. The first target consisted of two WB_2 and WB_4 phases. The second target was a nanocomposite of WB_4, WB_2, and TiB_2 phases. Detailed information about the manufacturing process and the chemical structure and mechanical properties of targets were described in Refs. [23] and [4], respectively. Based on our earlier studies on sputtering power and gas pressure [11], substrate temperature [10], and composition [4], the optimal parameters of deposition were chosen. The one-inch diameter target was mounted in the water-cooled magnetron sputtering cathode (Kurt J. Lesker, Jefferson Hills, PA, USA) and positioned at a distance of 50 mm in front of the target. The RF sputtering power was 50 W and bias potential on the substrate was floating. The deposition process occurred in a vacuum chamber initially pumped to 0.02 Pa and then filled with argon to a working pressure of 0.9 Pa. The gas flow of argon was 19 mL/min. Prior to each deposition, the target was sputtered for 5 min in order to ensure a clean surface and stable sputtering conditions. Film was deposited for 120 min on flat, polished substrate cut from WC rod (1 mm thick, Ø = 15 mm diameter; Stjorsen Polska, Tychy, Poland) and on commercial WC cutting tools. Before deposition, all substrates were cleaned with subsequent rinses in acetone, alcohol, and deionized water. Both substrates were mounted on a rotating holder and heated to 540 °C.

The crystal structure of the coating was investigated by X-ray diffraction (XRD) using Bruker D8 Discover (Cu radiation, λ = 1.5418 Å, Coventry, UK). Film measurement was taken in 2θ scan mode, with the source fixed at 8° position, which avoided signal from the substrate while maintaining high intensity of the signal originating primarily from the coating.

The surface was investigated with scanning electron microscopy (SEM; JEOL JSM6010PLUS/LV, Tokyo, Japan). Energy dispersive X-ray spectroscopy (EDS; JEOL (EUROPE) SA, Warszawa, Poland) microanalysis was used to study the elemental distribution. During EDS measurement, accelerating voltage of 7 kV was used. Due to problems with boron measurement and subsequently determining its quantity in combination with other, especially heavy elements, before measurement, the EDS spectrometer was calibrated based on polished W_2B_5 commercial standard (Huizhou Tian Yi Rare Material Co, Guang Dong, China, 99.9% purity).

Vickers microhardness tests were performed under 20 g load on a Hanneman tester (Zeiss, Jena, Germany). Five imprints were done on each tested sample. To evaluate film hardness, the substrate hardness was taken into account.

Surface roughness was measured on a Talysurf stylus scanning profilometer (Taylor Hobsson, Leicester, UK) according to ISO standards. The tip radius was 2 μm, traverse length according to ISO 4288 [24] was 1.25 mm, and cut-off was 0.25 mm. A standardized phase-correct Gaussian high-pass filter (ISO 11562 [25]) was applied. The profiles and surface measurements were done before and after the deposition process.

Wear tests were done on a Skoda–Savin tester (Skoda Works, Plzeň, Czech Republic) in semi-dry conditions. The test allows determination of wear at the semi-dry sliding friction. Determination of wear was made during rotational movement of the counter-sample made of WC–Co alloy sliding on a stationary sample while wetting the surface with cooling fluid. The following wear processes may occur: abrasion, chipping, surface plastic deformation, and adhesion. Figure 1 shows the scheme of the wear test.

The roller was pressed against the tested surface at constant load of 15 kg. Relative motion speed was 1.5 m/s. Preliminary tests showed that after 500 rotations, the depth of the worn area was less than 1 μm, so each test was stopped after 500 rotations, corresponding to the length of the friction span of 170 m. The coolant, 0.05% K_2CrO_4 solution in distilled water, was applied with flow efficiency of 1 L/min. Five tests were performed on each tested surface. After the tests, surface topography was studied by laser confocal microscopy (Keyence VK-X100, Osaka, Japan) and the volume of worn material was determined.

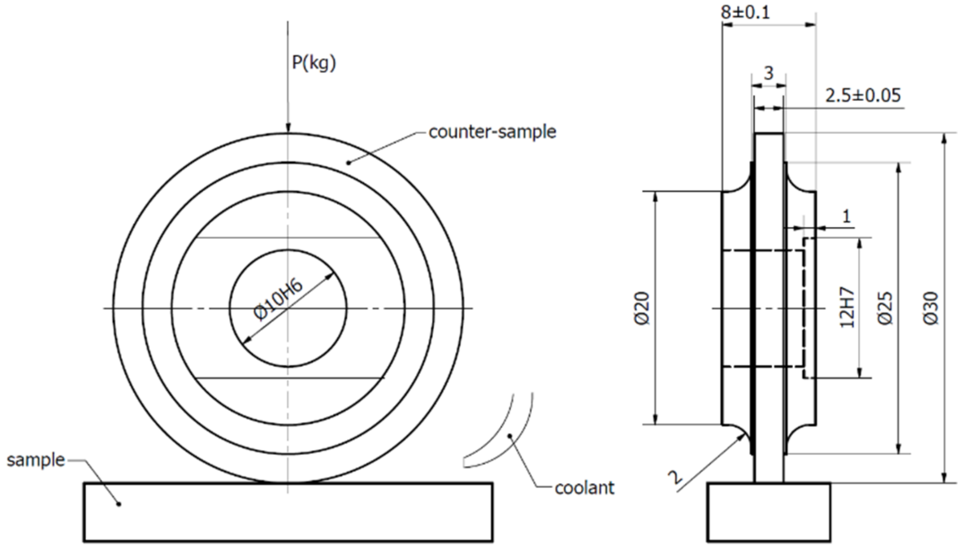

Figure 1. Stand for determination of wear at sliding friction.

The cutting test was performed on a Haas CNC TL1 lathe (Haas Automation, Oxnard, CA, USA). The turning process was performed on AISI 304 stainless steel. The constant cutting length was 70 mm and the following process parameters were applied: cutting speed v_c = 80 m/min, cutting depth a_p = 1.5 mm, and feed rate p = 0.09 mm/rev. Two commercially produced cemented carbide (WC–Co) cutting tool inserts, supplied by Sandvik Polska Sp. z o.o. (Warsaw, Poland), were tested with and without deposited coatings. Nominal composition of inserts was 94% WC and 6% Co (H13A). Five tests were performed on each insert. The insert was rotated about 70° to perform the next test. The cutting tool with marked test location is illustrated in Figure 2. After the cutting tests, the wear of inserts was observed by laser confocal microscopy and flank wear V_B was determined.

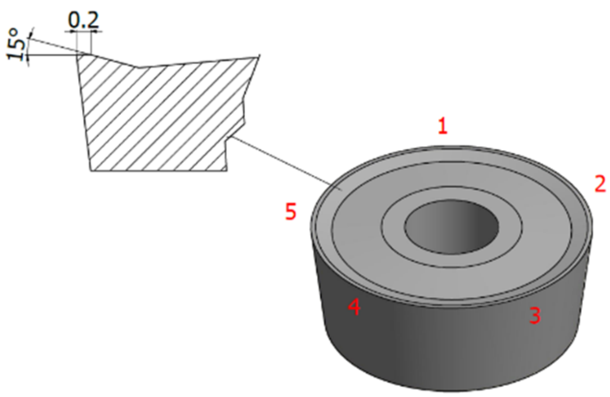

Figure 2. Cutting tool with marked test location [26] (adapted from sandvik.coromant.com).

3. Results and Discussion

3.1. Microstructure

The topography and chemical composition of deposited coating surface are presented in Figure 3. Both films were smooth with single impurities. EDS analysis (Figure 3) showed that all elements were uniformly distributed. As it is shown on exemplary distribution of tungsten (Figure 3a,b), there is no the micro-segregation of elements.

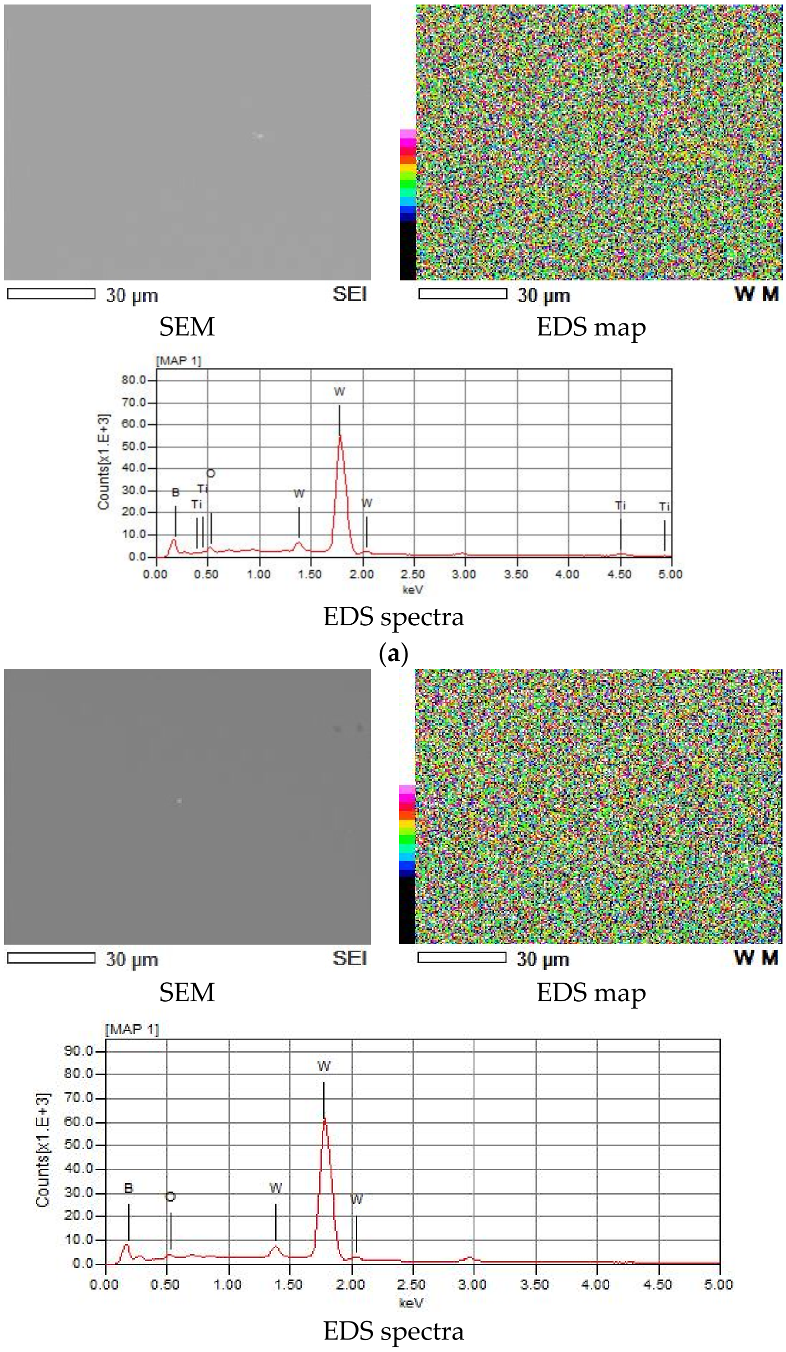

Figure 3. Chemical composition of (**a**) W-Ti-B and (**b**) W-B film based on SEM + EDS analysis of deposited coatings. The colored map presents distribution of tungsten.

Table 1 shows the chemical composition of deposited coatings. The addition of titanium caused a decrease in tungsten from 28.7 at.% to 23.1 at.%. However, it also changed the amount of oxygen from 4.1 at.% to 5 at.% and boron from 67.2 at.% to 68.3 at.%. A significant decrease in the amount of boron atoms in the deposited layers (B/(W + Ti) = 2.57) compared with the targets (4.5) can be explained by the reflection and scattering of the light element as a result of collisions with tungsten, which has an atomic mass 17 times greater [16]. Substitution of heavy tungsten by titanium causes more boron to reach the substrate, which is confirmed by the composition of the deposited layers (Table 1). In the case of oxygen, which possesses very high chemical activity [27], an increased amount is insignificant. It indicates that titanium can be in solid solution with crystal lattice of WB_2. Taking into consideration that in the low-temperature region under equilibrium conditions only 2% of titanium can be in solid solution with WB_2 lattice [28], the deposited coatings consist also of nanocomposite mixture of WB_2 and TiB_2. Such a hypothesis can be confirmed by XRD (Figure 4) and XPS studies, which were interpreted in more detail by Moscicki et al. [4].

Table 1. Composition of deposited coatings.

Composition	WB_y		$W_{1-x}Ti_xB_y$	
	Mass %	**Atom %**	**Mass %**	**Atom %**
B	12.0	67.2	14.1	68.3
W	86.9	28.7	81.1	23.1
Ti	0	0	3.2	3.5
O	1.1	4.1	1.6	5.1
y = B/(W + Ti)	–	2.3	–	2.6
x = Ti/(W + Ti)	–	0	–	0.1

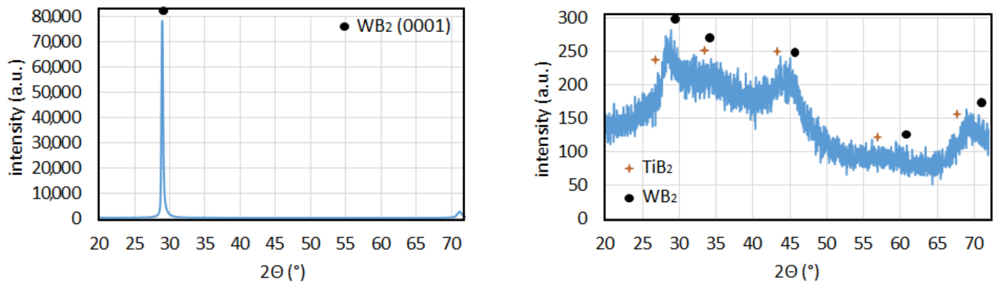

(**a**) (**b**)

Figure 4. X-ray diffraction patterns of deposited coatings: (**a**) columnar crystalline WB_2; (**b**) amorphous/ nanocrystalline $(W,Ti)B_2$.

As shown in Figure 4, the addition of titanium changed the structure of deposited coatings from crystalline (Figure 4a) to amorphous (Figure 4b). The only reflection (0001) at angle $2\theta = 28°$ indicates a strongly oriented columnar structure of WB_2. The addition of Ti resulted in the appearance of a second nanocrystalline phase. Investigations on diborides show that those materials prefer to crystallize mainly in two related hexagonal structures: AlB_2 structure type P6/mmm, preferably formed by titanium diborides, or W_2B_{5-x}-based structure P63/mmc, favored by WB_2 [29]. However, vacancies, which are typical for magnetron sputtered materials, are beneficial for stabilizing the α-structure [29]. Additionally, the formation enthalpy is lower for α- than ω-structure for high Ti content, which promotes rebuilding of P63/mmc to P6/mmm structure and consequent amorphization of coating. The X-ray diffraction patterns of nanocrystalline $(W,Ti)B_2$ coating can be seen in Figure 4b. Such a change increases the fracture toughness [14,20] but does not affect the very high hardness of deposited films.

3.2. Surface Topography

The thickness of the coatings was measured in a stepwise manner on polished samples by confocal microscope. It was seen that the thickness of W–B film was 1.81 ± 0.11 µm and W–Ti–B film was 1.43 ± 0.15 µm. Surface was smooth with single impurities.

Surface roughness was measured on flat polished samples and on cutting inserts before and after the deposition process. The surface topography of the substrate is still noticeable after the deposition process. Deposited films covered the substrate, keeping the shape of the roughness.

Roughness parameters are shown in Table 2. After deposition, the average value of the height of roughness (R_a, R_q), maximum profile valley depth (R_v), maximum height of profile (R_z) and maximum height of peaks (R_p) increases for both films. This is related to the presence of single impurities on the surface after deposition. Spatial parameter S_m does not change and corresponds to the distribution of carbides on the substrate.

Table 2. Profile of roughness parameters, cut-off 0.25 mm.

Roughness Parameters (µm)	WC	W–B	W–Ti–B
R_a	0.022	0.029	0.038
R_q	0.026	0.036	0.043
R_p	0.069	0.119	0.096
R_v	0.066	0.089	0.090
R_z	0.134	0.208	0.145
S_m	5.4	6.3	4.5

The topography of the surface can be better revealed by 3-D surface roughness measurement. Figure 5 shows surface topography measured on a scanning profilometer. Waviness related to polishing process is observed for each sample. In the case of W–Ti–B coating, more impurities are visible as picks (Figure 5c) and the value of area roughness S_a, surface roughness height of peaks S_p and valley S_v, as well as maximum height S_z (Table 3), are bigger than for WC–Co and W–B film, similar to the profile parameters.

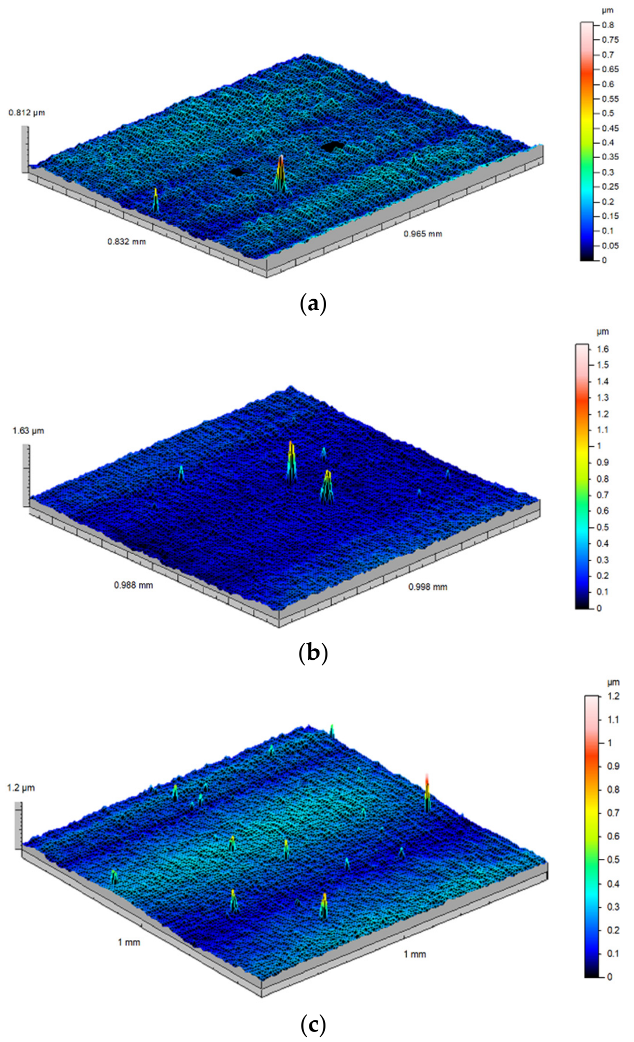

Figure 5. Surface topography of (**a**) WC–Co, (**b**) W–B film, (**c**) W–Ti–B film (scanning profilometer).

Table 3. Surface roughness parameters without filtration.

Roughness Parameters (μm)	WC	W–B	W–Ti–B
S_a	0.026	0.045	0.043
S_p	0.667	1.470	1.010
S_v	0.144	0.166	0.208
S_z	0.809	0.906	0.925

The profile roughness measurement was also done on cutting tools. Figure 6 shows the topography of the surface of cutting inserts observed on confocal microscope without and with deposited W–B film. In the case of WC–Co insert, small carbides in the matrix with characteristic sharp shape for WC grains were observed (Figure 6a). After deposition of W–B coating, the surface morphology changed, however single carbides were still observed (Figure 6b).

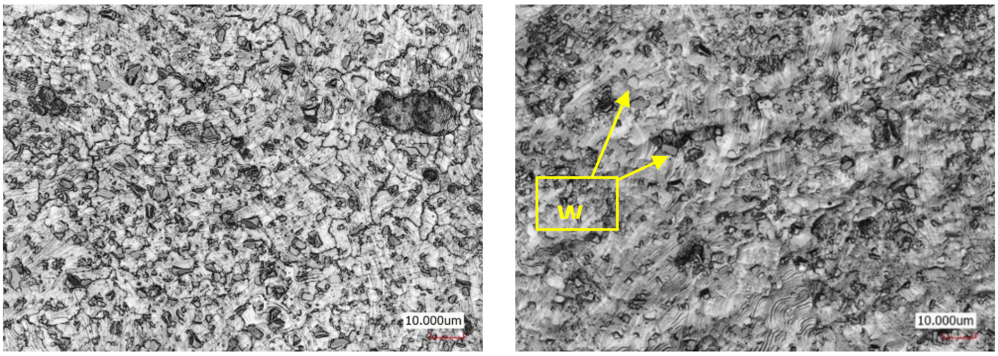

(**a**) (**b**)

Figure 6. Surface topography of (**a**) cutting insert WC–Co, (**b**) insert with deposited W-B film.

The average value of profile roughness height (R_a, R_q) and maximum height R_z of the peak are smaller after the deposition process. Deposited material is located on the roughness valley, causing a smaller value of parameter R_v (Table 4) compared to the uncoated insert.

Table 4. Roughness parameters of cutting tools, cut-off 0.25 mm.

Insert	Roughness Parameters (μm)			
	R_a (μm)	R_z (μm)	R_q (μm)	R_v (μm)
WC–Co	0.43	3.00	0.55	1.46
W–B	0.32	2.30	0.41	1.14

3.3. Microhardness

Microhardness tests showed that for the sample with W–B coating deposited on WC–Co substrate, the hardness value was 2680 $HV_{0.02}$, with standard deviation of 360. As a result that the depth of imprints was about 0.35 μm, it was necessary to take into account the hardness of the substrate to evaluate the hardness of the film. Based on the formula in [30] and substrate hardness 2000 $HV_{0.02}$, the hardness of the W-B film was estimated at 2960 ± 440 $HV_{0.02}$. This value is close to the one obtained for a similar coating presented in [9]. The sample with W–Ti–B coating was harder (2810 ± 130 $HV_{0.02}$) and estimated hardness of the film without the influence of substrate was 3630 ± 260 $HV_{0.02}$. The increased hardness of titanium alloyed coatings can be related to different mechanisms, e.g., solid solution hardening [31] or precipitation hardening [32]. In the case of W–Ti–B nanocomposite, which consists of coherently coupled grains of two phases with a hexagonal crystal structure (α-WB_2 and TiB_2), the binding strength is increased. According to XRD studies (Figure 4), such a composite is formed during RF magnetron sputtering. The creation of coherent boundaries between the crystallites of different phases increases the hardness of the composite. The formation of such boundaries between grains causes suppression of grain-boundary sliding in nanocrystalline materials [15]. This leads to increased film strength and hardness.

3.4. Wear Test

Wear test was performed for WC–Co flat samples with W–B and W–Ti–B coatings. Results were compared with wear resistance of WC–Co samples without coating. After testing the surface of samples, a groove was observed. For WC–Co samples, 1.9 µm groove depth was noted. Figure 7a shows an example of worn groove on W–B coating. In this case, the maximum depth of grooves after the wear test was 1.4 µm, which was less than the thickness of the film (1.8 µm). Figure 7 shows that the surface of the grooves was smooth with some irregularities on boundary, with unworn material. In the case of W–Ti–B film, cracks were observed on the groove boundary (Figure 8b). Table 5 shows the volume of lost material for tested samples after wear tests measured with confocal microscope and calculated based on the analysis program.

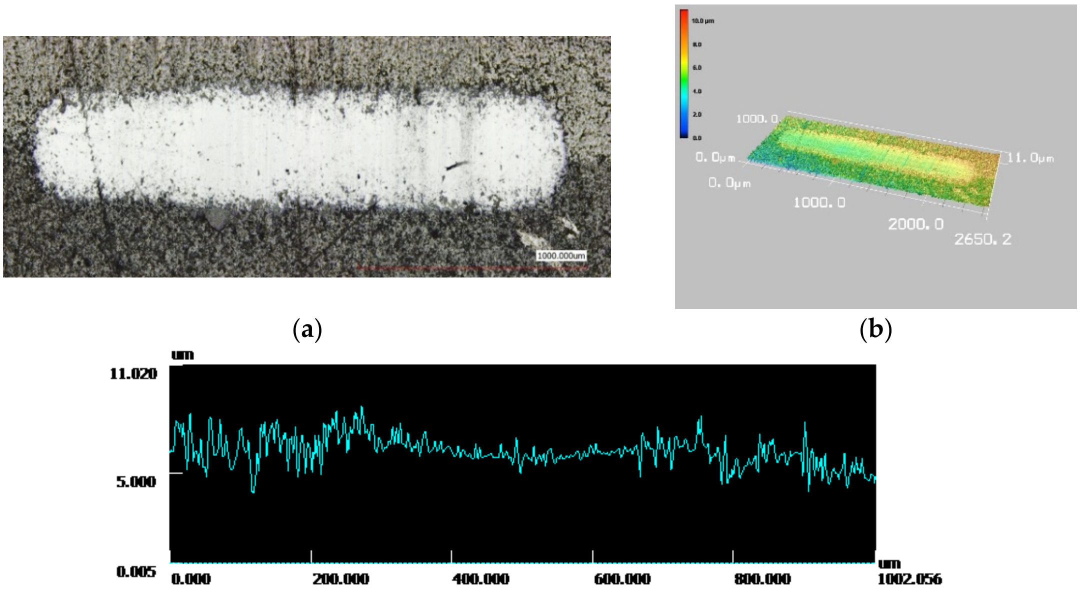

(**a**) (**b**) (**c**)

Figure 7. (**a**) Sample groove after wear test; (**b**) 3D-view; (**c**) profile perpendicular to longer axis: W–B coating.

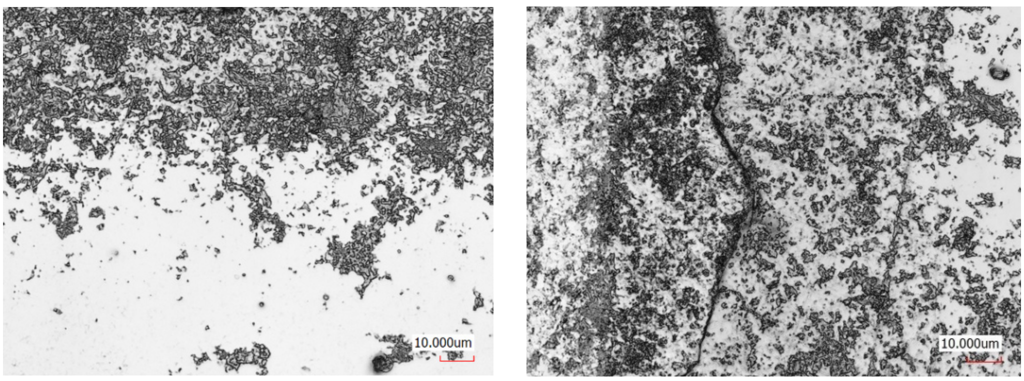

(**a**) (**b**)

Figure 8. Boundary of worn zone: (**a**) W–B coating, (**b**) W–Ti–B coating.

Table 5. Volume of loss material after wear tests.

Sample Material	Volume of Loss Material (10^6 μm^3)					Mean Value
	1	2	3	4	5	
WC–Co	1.06	0.941	1.217	1.089	0.978	1.057
W–B film on WC–Co	0.598	0.466	0.496	1.011	0.620	0.638
W–Ti–B film on WC–Co	1.106	0.897	1.276	1.197	1.820	1.259

The highest wear resistance was noted for the sample with W–B film. The volume of lost material was about 40% less than for the uncoated WC–Co sample. In the case of W–Ti–B film, wear resistance was the worst and even lower than the uncoated sample.

Microscopic observation of worn areas revealed that the W–B film surface was smooth without cracks. Figure 8a shows a boundary area without cracks and other imperfections. Results indicated that abrasive wear was a dominant process in this case. For the W–Ti–B film, cracks and delamination of coating were observed on groove boundaries (Figure 8b). This phenomenon can explain the higher material loss of W–Ti–B film compared to other samples and the varying values of the volume loss of material in this case. Very hard delaminated fragments of the films can accelerate wear before they are removed from the treatment zone by the coolant.

3.5. Turning Test

Cutting test was performed for WC–Co insert and for insert with W–B coating. After the cutting tests, the inserts were investigated by laser confocal microscopy. Wear was measured on the flank of the insert and the flank wear V_B was determined. For both tested inserts, smooth abrasive wear was observed. Figure 9 shows cutting edges after the test. Flank wear was less for W–B coated inserts (Figure 9a) than for WC–Co inserts (Figure 9d). The detailed observation reveals additional wear mechanisms that are different for each tool. Figure 9b,c show adherent material. Figure 9c shows a profile of the cutting edge after machining. A change in insert geometry caused by build-up was observed in both cases. This mechanism is caused by pressure welding of the chip to the insert. It is most common during machining of sticky materials with low cutting speed. To prevent this kind of wear, the highest speed should be applied.

For the WC–Co insert, flank wear was combined with chipping of the cutting edge visible on Figure 9e,f. This mechanical wear is more dangerous than adhesive wear and can lead to rapid tool failure.

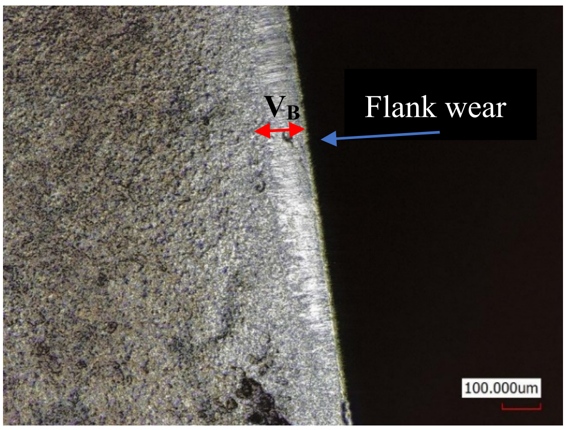

(**a**)

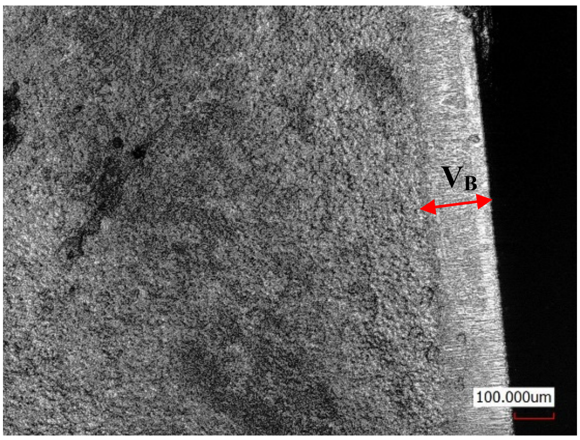

(**d**)

Figure 9. *Cont.*

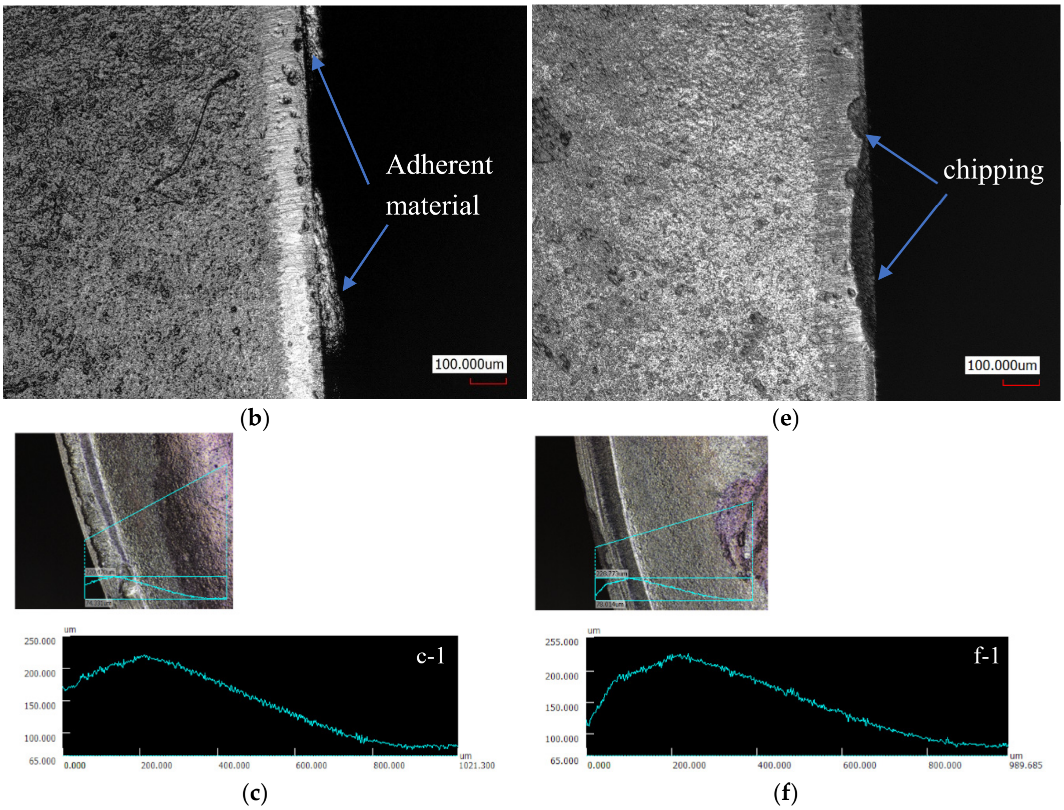

Figure 9. Wear of cutting edge: (**a**–**c**) WC–Co insert with W-B coating; (**d**–**f**) WC–Co. (**c-1**): enlarged insert (chart) from Figure 9c; (**f-1**): enlarged insert (chart) from Figure 9f.

Table 6 shows measurement results of the mean value of flank wear V_B for a constant cutting length of 70 mm. Wear of the insert with W–B film was smaller than 30% compared to uncoated insert (Figure 10). That is compatible with the results of the wear test, in which 40% less volume of material was found (Table 5).

Table 6. Results of flank wear V_B after turning test for WC–Co insert and W–B coated insert.

No Test	**V_B (µm)**	
	WC–Co	**W–B Film**
1	160	104
2	184	103
3	172	145
4	218	115
5	167	141
Mean value	180	122
Std. dev.	22.9	20.1

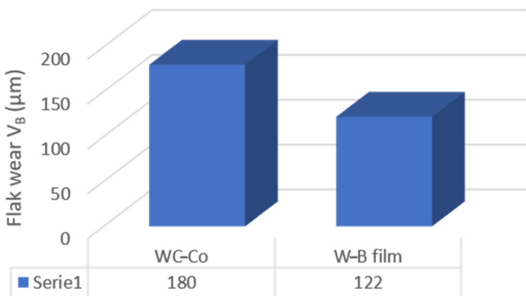

Figure 10. Flank wear V_B of cutting edges WC–Co and WC–Co coated with W–B film after turning tests at constant cutting conditions v_c = 80 m/min, a_p = 1.5 mm, p = 0.09 mm/rev and cutting length 70 mm.

4. Conclusions

In this work, properties of boride coatings such as WB_x and $(W,Ti)B_2$ deposited by RF magnetron sputtering and the possibility of using them to protect WC–Co cutting tools for difficult-to-machine materials are described. The main conclusions are as follows:

- W–B and W–Ti–B coatings deposited on WC–Co substrate are smooth and very hard. However, titanium alloy films with hardness of 3630 ± 260 $HV_{0.02}$ are characterized by lower adhesion to the substrate, which influences the wear mechanism.
- The wear test at semi-dry sliding friction revealed 40% better wear resistance for W–B coating compared to WC–Co and W–Ti–B coating. In case of the W–Ti–B film, delamination and cracking were noted.
- In the turning test of difficult-to-cut 304 stainless steel, the W–B coated tool showed better wear resistance than the uncoated tool.
- Flank wear was smaller by 30% when W–B film was applied, compared to uncoated WC–Co insert. Additionally, coating prevented chipping of the edge during cutting in tested conditions.
- W–B film deposited by magnetron sputtering has great potential as a coating for cutting tools for difficult-to-cut materials, but it is necessary to carry out more tests under various cutting conditions.

Author Contributions: Conceptualization, J.R. and T.M.; methodology, J.R. and R.P.; investigation, J.R. and T.M.; data curation, J.R. and T.M.; writing—original draft preparation, J.R.; writing—review and editing, T.M. All authors have read and agreed to the published version of the manuscript.

Funding: This work was supported by the National Science Centre, Poland (Grant No. 2017/25/B/ST8/01789).

Conflicts of Interest: The authors declare no conflict of interest.

References

1. Yumashev, A. Mikhaylov Development of polymer film coatings with high adhesion to steel alloys and high wear resistance. *Polym. Compos.* **2020**, *41*, 2875–2880. [CrossRef]
2. Fuger, C.; Moraes, V.; Hahn, R.; Bolvardi, H.; Polcik, P.; Riedl, H.; Mayrhofer, P.H. Influence of Tantalum on phase stability and mechanical properties of WB_2. *MRS Commun.* **2019**, *9*, 375–380. [CrossRef]
3. Alishahi, M.; Mirzaei, S.; Souček, P.; Zábranský, L.; Buršíková, V.; Stupavská, M.; Peřina, V.; Balázsi, K.; Czigány, Z.; Vašina, P. Evolution of structure and mechanical properties of hard yet fracture W–B–C coatings with varying C/W ratio. *Surf. Coat. Technol.* **2018**, *340*, 103–111. [CrossRef]
4. Moscicki, T.; Psiuk, R.; Slominska, H.; Levintant-Zayonts, N.; Garbiec, D.; Pisarek, M.; Bazarnik, P.; Nosewicz, S.; Chrzanowska-Giżyńska, J. Influence of overstoichiometric boron and titanium addition on the properties of RF magnetron sputtered tungsten borides. *Surf. Coat. Technol.* **2020**, *390*, 125689. [CrossRef]
5. Chrzanowska, J.; Hoffman, J.; Denis, P.; Giżyński, M.; Mościcki, T. The effect of process parameters on rhenium diboride films deposited by PLD. *Surf. Coat. Technol.* **2015**, *277*, 15–22. [CrossRef]
6. Wicher, B.; Chodun, R.; Trzciński, M.; Lachowski, A.; Kubiś, M.; Nowakowska-Langier, K.; Zdunek, K. Design of pulsed neon injection in the synthesis of W–B–C films using magnetron sputtering from a surface-sintered single powder cathode. *Thin Solid Film.* **2020**, *716*, 138426. [CrossRef]
7. Berger, M.; Coronel, E.; Olsson, E. Microstructure of d.c. magnetron sputtered TiB_2 coatings. *Surf. Coat. Technol.* **2004**, *185*, 240–244. [CrossRef]
8. Pierson, J.; Belmonte, T.; Michel, H. Low temperature growth mechanisms of zirconium diboride films synthesised in flowing microwave Ar–BCl_3 post discharges. *Surf. Coat. Technol.* **1999**, *116–119*, 1049–1054. [CrossRef]
9. Dearnley, P.; Schellewald, M.; Dahma, K. Characterisation and wear response of metal-boride coated WC–Co. *Wear* **2005**, *259*, 861–869. [CrossRef]
10. Chrzanowska-Giżyńska, J.; Denis, P.; Woźniacka, S.; Kurpaska, Ł. Mechanical properties and thermal stability of tungsten boride films deposited by radio frequency magnetron sputtering. *Ceram. Int.* **2018**, *44*, 19603–19611. [CrossRef]
11. Chrzanowska, J.; Kurpaska, Ł.; Giżyński, M.; Hoffman, J.; Szymański, Z.; Mościcki, T. Fabrication and characterization of superhard tungsten boride layers. *Ceram. Int.* **2016**, *42*, 12221–12230. [CrossRef]
12. Jiang, C.; Pei, Z.; Liu, Y.; Xiao, J.; Gong, J.; Sun, C. Preparation and characterizationof superhard AlB_2-type WB_2 nanocomposite coatings. *Phys. Status Solidi A* **2013**, *210*, 1221–1227. [CrossRef]

13. Paiva, J.; Shalaby, M.; Chowdhury, M.; Shuster, L.; Chertovskikh, S.; Covelli, D.; Junior, E.L.; Stolf, P.; Elfizy, A.; Brok, C.S.; et al. Tribological and wear performance of carbide tools with TiB_2 PVD coating under varying machining conditions of $TiAl_6V_4$ aerospace alloy. *Coatings* **2017**, *7*, 187. [CrossRef]
14. Euchner, H.; Mayrhofer, P.; Riedl, H.; Klimashin, F.; Limbeck, A.; Polcik, P.; Kolozsvari, S. Solid solution hardening of vacancy stabilized $Ti_xW_{1-x}B_2$. *Acta Mater.* **2015**, *101*, 55–61. [CrossRef]
15. Sobol, O.; Dub, S.; Pogrebnjak, A.; Mygushchenko, R.; Postelnyk, A.; Zvyagolsky, A.; Tolmachova, G. The effect of low titanium content on the phase composition, structure, and mechanical properties of magnetron sputtered WB_2–TiB_2 films. *Thin Solid Film.* **2018**, *662*, 137–144. [CrossRef]
16. Chrzanowska-Giżyńska, J.; Denis, P.; Giżyński, M.; Kurpaska, Ł.; Mihailescu, I.; Ristoscu, C.; Szymański, Z.; Mościcki, T. Thin WB_x and $W_yTi_{1-y}B_x$ films deposited by combined magnetron sputtering and pulsed laser deposition technique. *Appl. Surf. Sci.* **2019**, *478*, 505–513. [CrossRef]
17. Wang, H.; Wang, B.; Li, S.; Xue, Q.; Huang, F. Toughening magnetron sputtered TiB_2 coatings by Ni addition. *Surf. Coat. Technol.* **2013**, *232*, 767–774. [CrossRef]
18. Newirkowez, A.; Cappi, B.; Telle, R.; Schmidt, H. $(Ti,W,Cr)B_2$ coatings produced by dc magnetron sputtering. *Thin Solid Film.* **2012**, *520*, 1775–1778. [CrossRef]
19. Sobol, O.; Grigoryev, O.; Kunitsky, Y.; Dub, S.; Podtelezhnikov, A.; Stetsenko, A. Peculiarities of structure state and mechanical characteristics in ion-plasma condensates of quasibinary system borides W_2B_5–TiB_2. *Sci. Sinter.* **2006**, *38*, 63–72. [CrossRef]
20. Smolik, J.; Kacprzńska-Gołacka, J.; Sowa, S.; Piasek, A. The analysis of resistance to brittle cracking of tungsten doped TiB_2 coatings obtained by magnetron sputtering. *Coatings* **2020**, *10*, 807. [CrossRef]
21. Smolik, J.; Mazurkiewicz, A.; Garbacz, H.; Kopia, A. Tungsten doped TiB_2 coatings obtained by magnetron sputtering. *J. Mach. Constr. Maint.* **2018**, *4*, 27–32.
22. Musil, J. Flexible hard nanocomposite coatings. *RSC Adv.* **2015**, *5*, 60482–60495. [CrossRef]
23. Moscicki, T.; Radziejewska, J.; Hoffman, J.; Chrzanowska, J.; Levintant-Zayonts, N.; Garbiec, D.; Szymanski, Z. WB_2 to WB_3 phase change during reactive spark plasma sintering and pulsed laser ablation/deposition processes. *Ceram. Int.* **2015**, *41*, 8273–8281. [CrossRef]
24. *ISO 4288 Geometrical Product Specifications (GPS)—Surface Texture: Profile Method—Rules and Procedures for the Assessment of Surface Texture*; International Organization for Standardization (ISO): Geneva, Switzerland, 1 August 1996.
25. *ISO 11562 Geometrical Product Specifications (GPS)—Surface Texture: Profile Method—Metrological Characteristics of Phase Correct Filters*; International Organization for Standardization (ISO): Geneva, Switzerland, 1 December 1996.
26. T-Max® P Insert for Turning RCMX 12 04 00 H13A (SANDVIK Coromant). Available online: https://www.sandvik.coromant.com/en-gb/products/pages/productdetails.aspx?c=rcmx%2012%2004%2000%20h13a (accessed on 15 December 2020).
27. Humphrey, G.L. The heats of formation of TiO, Ti_2O_3, Ti_3O_5 and TiO_2 from combustion calorimetry. *J. Am. Chem. Soc.* **1951**, *73*, 1587–1590. [CrossRef]
28. Shovkoplyas, O.A.; Sobol, O.V. Influence of thermal and radiation effects on the phase composition, structure and stress-strain state of Ti–W–B system coatings deposited from ion-atomic fluxes. *J. Nano-Electron. Phys.* **2014**, *6*, 02024.
29. Moraes, V.; Riedl, H.; Fuger, C.; Polcik, P.; Bolvardi, H.; Holec, D.; Mayrhofer, P. Ab initio inspired design of ternary boride thin films. *Sci. Rep.* **2018**, *8*, 9288. [CrossRef]
30. Jonsson, B.; Hogmark, S. Hardness measurement of thin films. *Thin Solid Film.* **1984**, *114*, 257–269. [CrossRef]
31. Zhao, F.; Tao, Q.; You, C.; Ye, M.; Li, L.; Han, Y.; Dong, S.; Wang, X.; Cui, T.; Zhu, P. Enhanced hardness in tungsten–substituted molybdenum diboride solid solutions by local symmetry reduction. *Mater. Chem. Phys.* **2020**, *251*, 123188. [CrossRef]
32. Bakhit, B.; Palisatis, J.; Wu, Z.; Sortica, M.; Primetzhofer, D.; Persson, P.; Rosen, J.; Hultman, L.; Petrov, I.; Greene, J.; et al. Age hardening in superhard ZrB_2-rich $Zr_{1-x}Ta_xB_y$ thin films. *Scr. Mater.* **2021**, *191*, 120–125. [CrossRef]